Materials Transactions, Vol. 44, No. 10 (2003) pp. 1900 to 1911
Special Issue on Nano-Hetero Structures in Advanced Metallic Materials

OVERVIEW

Nanocrystallization of Steels by Severe Plastic Deformation

Minoru Umemoto

Department of Production Systems Engineering, Toyohashi University of Technology, Toyohashi 441-8580, Japan

The formation of nanocrystalline structure (NS) in steels by various severe plastic deformation processes, such as ball milling, a ball drop test, particle impact deformation and air blast shot peening are demonstrated. Layered or equiaxed nanograined region appeared near the specimen surface and dislocated cell structured region appeared interior of specimens. These regions are separated with clearly defined boundaries. The deformation induced nanograined regions have the following common specific characteristics: 1) with grains smaller than 100 nm and low dislocation density interior of grains, 2) extremely high hardness, 3) dissolution of cementite when it exist and 4) no recrystallization and slow grain growth by annealing. The deformation conditions to produce NS was discussed based on the available data in literatures. It was suggested that the most important condition is to impose a strain larger than about 7. High strain rates, low deformation temperature, multidirectional deformation, hydrostatic pressure are considered to be favorable conditions to produce NS. Introducing alloying elements, precipitates and second phase also enhance nanocrystallization by suppressing recovery. The mechanisms of the formation of sharply defined boundaries which separate nanograined structure region from dislocated cell structured region were discussed with respect to impurities, martensitic transformation and deformation. It was suggested several mechanisms may operate simultaneously in the formation of the clear boundaries.

(Received May 30, 2003; Accepted July 24, 2003)

Keywords: *ball mill, ball drop, shot peening, nanocrystallne, microstructure, severe deformation, steel*

1. Introduction

Large efforts have been devoted to refine grains of materials since it enhances both strength and toughness. Figure 1 shows various processes to produce fine grained materials of respective grain size ranges. In steel industry, thermomechanical control processing (TMCP),[1] which consists of controlled hot rolling and accelerated cooling, has been developed to produce fine grained materials with grain size down to around 5 μm. In order to obtain the finer grains up to 1 μm extended TMCP processes have been developed.[2] In such processes, diffusional transformation and/or recrystallization were mainly utilized to refine grains. In the conventional deformation processes such as rolling, drawing, extrusion, further refinement of grains to less than 1 μm is quite difficult since the final product size limits the maximum amount of strain introduced. To eliminate the strain limit arising from the materials size reduction, new deformation processes such as Equal channel angular pressing (ECAP)[3–5] or accumulative roll bonding (ARB)[6,7] have been developed.

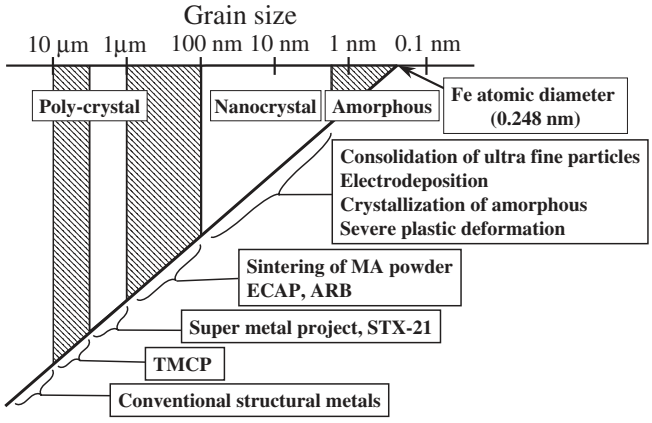

Fig. 1 Production methods of fine grained materials for respective grain size range.

In ECAP process, pure shear deformation is repeatedly imposed in materials without changing the cross-sectional dimensions of the workpiece. Bulk rod-like specimens with submicron size grains has been obtained. In ARB, two pieces of sheet specimen were stacked and rolled to 50% reduction. The obtained roll-bonded sheet was cut into half length and repeated such procedure by several cycles. Bulk sheet form specimens with submicron grains has been obtained.

To obtain nanograined materials (grain size smaller than 100 nm), various methods such as consolidation of ultrafine powders,[8] electron beam deposition,[9] electrodeposition,[10] crystallization of amorphous phase,[11] severe plastic deformation[12–24] *etc.* have been developed. Figure 2 shows representative severe plastic deformation processes to produce nanocrystalline structure (NS): ball milling,[12–15] high pressure torsion,[16,17] sliding wear,[18] a ball drop test,[19,20] ultrasonic shot peening[21] and air blast shot peening.[22–24] Figure 3 shows the reported Vicker's hardness ranges of various pure metals (includes specimens with a small amount of alloying elements) of nanometer sized grain (smaller than 100 nm, called nanograin hereafter) produced by various methods.[25,26] In the figure theoretically estimated hardness of selected grain sizes are also shown. The theoretical hardness value was calculated from Hall-Petch relationship using the equation $HV = HV_0 + 1.5\mu(b/d)^{1/2}$ (where μ is the shear modulus, b the Bergers vector and d the grain diameter). As is seen, the reported hardness of Al, Ti, Ni and Fe exceed the expected hardness of respective metals with 100 nm grain size except Cu.

In the present review the microstructure evolutions in steels by ball milling, a ball drop test, particle impact test and air blast shot peening are presented. Focusing on iron and steels, previous studies on the microstructural evolution during heavy deformation were reviewed. The amount of strain, strain rate and other favorable conditions to produce NS are discussed.

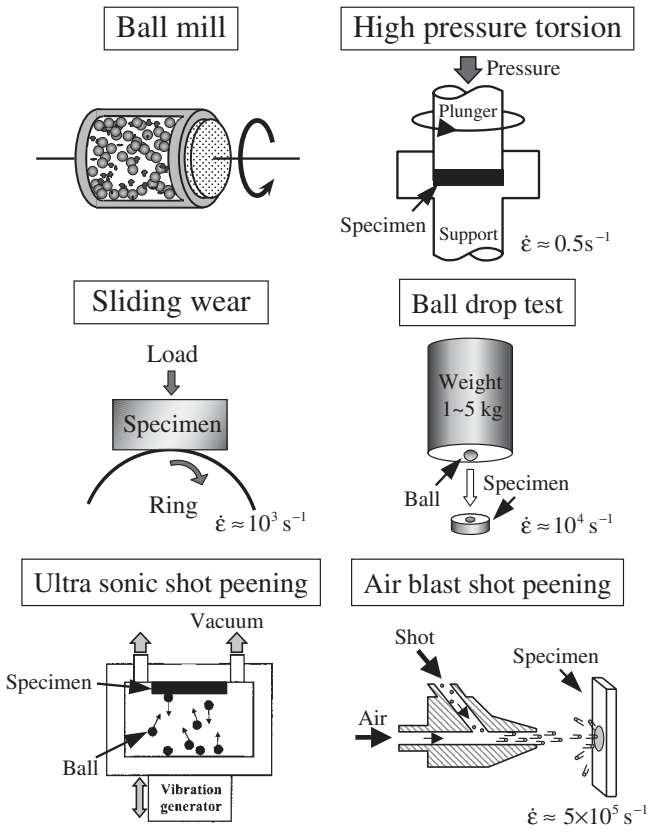

Fig. 2 Various severe plastic deformation processes to produce nanograined structure.

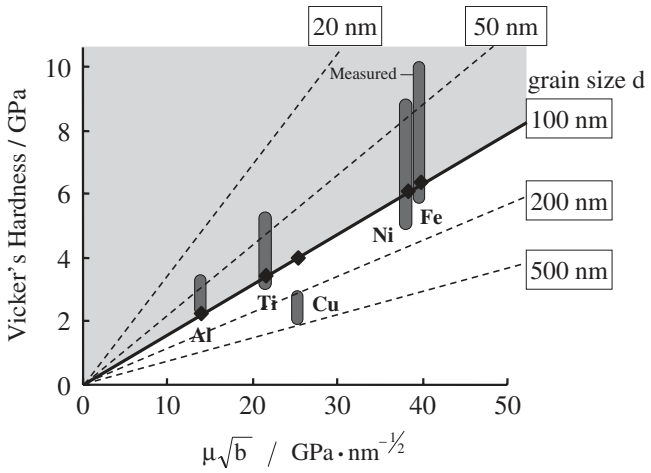

Fig. 3 Measured Vicker's hardness of nanograined (less than 100 nm) pure metals and theoretically estimated hardness of selected grain sizes.

2. Nanocrystallization in Steels by Various Plastic Deformation Processes

2.1 Nanocrystallization by ball milling

NS synthesized by ball milling was first reported in 1988 by Shingu *et al.*[12] in Al-Fe composite. Nanograined pure iron was first produced by Jang and Koch.[13] Using ball milling, they obtained nanometer sized grains down to 6 nm and Vicker's hardness up to 10 GPa. Grain refinement by ball milling to nano-meter range has been reported in various pure metals with bcc and hcp[14] and fcc[15] crystal structures.

Figure 4 shows SEM micrographs of the ball milled Fe-0.1C (in mass% hereafter) martensite with initial hardness of 3.2 GPa. From the full view of the cross section of a powder (Fig. 4(a)) two distinct regions are recognized. One is the dark uniform contrast region with several tens of μm thick observed near the surface of a powder and the another is the bright contrast region observed interior of the powder with deformed martensite morphology. The hardness of dark contrast region (8.8 GPa) is much higher than that of bright contrast region (3.9 GPa) as shown in Fig. 4 (b). The bright contrast region is in the conventinal work hardened state since the hardness of 3.9 GPa corresponds to that of same materials after 70% cold rolled. The boundaries between these two types of regions are clear and sharp. There is no intermediate structure between these two regions. The TEM observation of ball milled samples of various compositions (some are shown below) revealed that the dark contrast area corresponds to nanograined structured region and the bright contrast area corresponds to dislocated cell structured region, respectively. These two types of structures were observed in all the ball milled carbon steels irrespective of the carbon content (0 ~ 0.9 mass%C) or starting microstructure (ferrite, martensite, pearlite or spheroidite). Figure 5 shows the hardness distribution (measured by dynamic ultramicrohardness tester) across the two regions in ball milled pure iron. A drastic change in hardness from 7 to 3 GPa at the boundary of

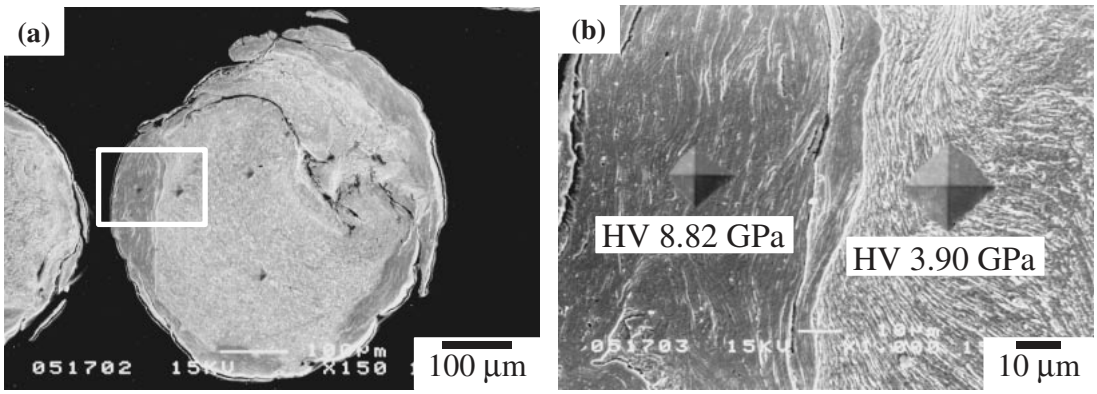

Fig. 4 SEM micrographs of Fe-0.10C martensite ball milled for 360 ks. (a) full view of a milled powder and (b) enlarged picture of (a) showing the hardness of nanocrystalline region (left hand side) and deformed structured region (right hand side) near powder surface.

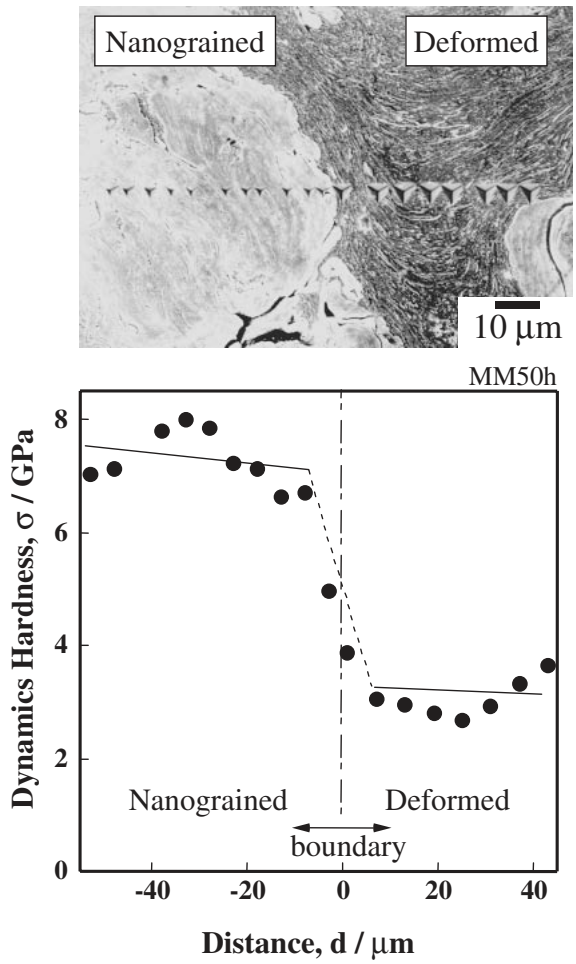

Fig. 5 Hardness distribution across the boundary between nanocrystalline region (left hand side) and deformed structured region (right hand side) of Fe-0.03C ball milled for 180 ks.

these two regions is seen. There is no transition region with intermediate hardness. With increasing milling time, the powder size reduced and the volume fraction of NS region increased. After a long time milling, powder is refined and entire area becomes NS.

The TEM micrographs of milled powder are shown in Figs. 6-9. Figure 6 shows the area around the boundary of two regions in the Fe-0.004C alloy. The layered nanocrystalline structure with an average thickness of about 100 nm (right hand side) and dislocated cell structure (left hand side) are seen. These two regions are separated with sharp boundary and there is no transition region. Figure 7 shows a high magnification of the layered nanostructure. It is seen that layered nanostructure consists of elongated grains with sharp grain boundaries. From the high resolution TEM observation, it was confirmed that deformation induced grain boundaries are high angle boundaries and contain many steps and facets.[27,28] Figure 8[27] shows the layered nanostructure in ball milled Fe-0.89C alloy with spheroidite structure. The thickness of the layers is around 20 nm which is much smaller than that of pure iron. The layers are subdivided into small grains as seen with different contrast. After milled for a long time uniformly distributed fine grains about 5-10 nm are produced (Fig. 9). These nanograins are randomly orientation as is seen from the continuous diffraction rings (Fig. 9).

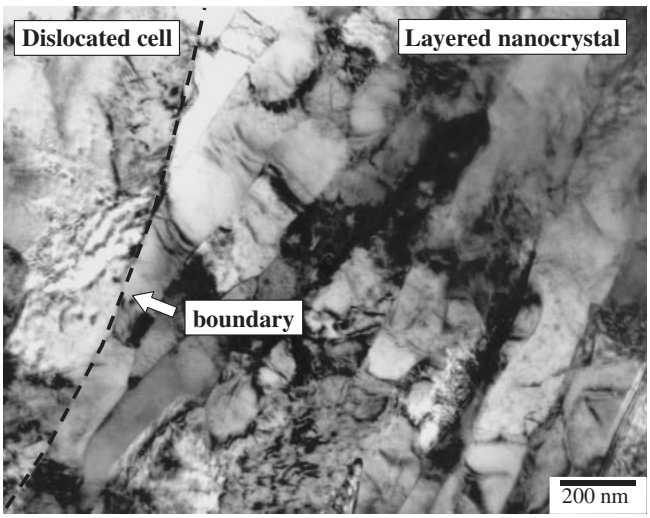

Fig. 6 TEM microstructure around the boundary between layered nanocrystalline region (left hand side) and dislocated cell structured region (right hand side) in Fe-0.004C ball milled for 360 ks.

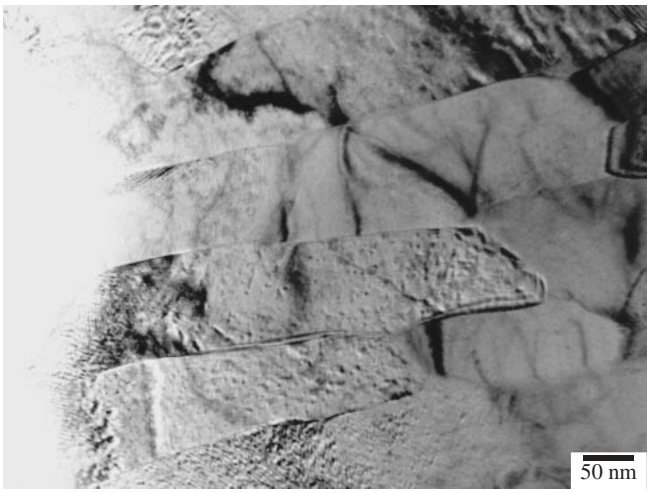

Fig. 7 TEM micrograph of the layered nanocrystalline region observed in Fe-0.004C ball milled for 360 ks.

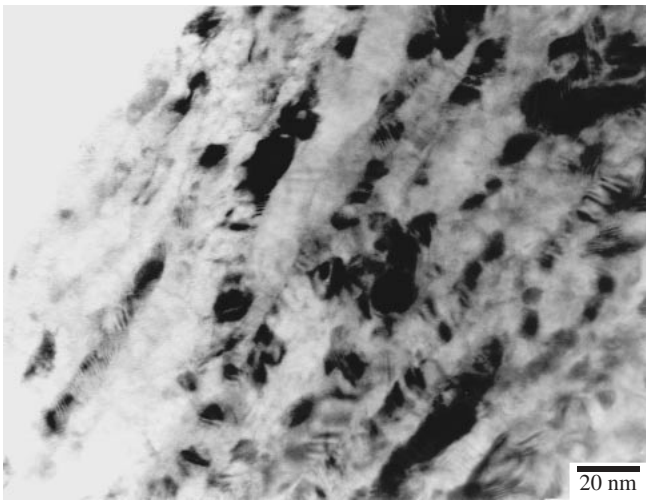

Fig. 8 TEM micrograph of the layered nanocrystalline region in Fe-0.89C spheroidite ball milled for 360 ks.

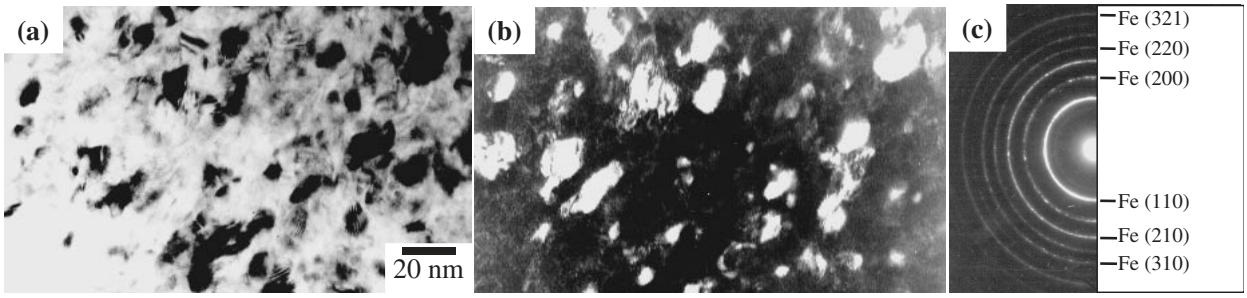

Fig. 9 High resolution TEM micrographs of Fe-0.89%C spheroidite after ball milled for 1800 ks. (a) bright field, (b) dark field and (c) diffraction pattern.

These observations suggest that randomly oriented equiaxed nanograins are produced by the subdivision of layers and rotation of divided regions. The diffuse contrast of equiaxed nanograin boundaries suggesting that they are highly disordered.

Figure 10[29] shows the hardness of NS and dislocated cell structured regions in ball milled powders as a function of carbon content. The hardness of both regions increases with carbon content. In the nanocrystalline region, the grain size decreased with carbon content. The increase in hardness with carbon content is considered to be mainly due to the decrease in grain size and partly due to the solution hardening of carbon. In the figure the hardness of as quenched martensite[30] is shown for comparison. It should be noted that the hardness of nanograined region is about 4 GPa higher than its martensite counterpart.

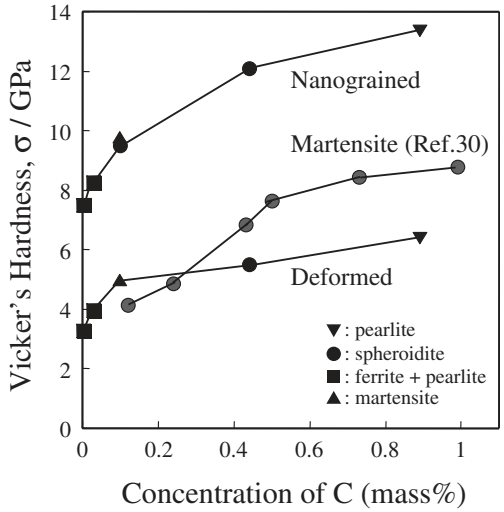

Fig. 10 Hardness of nanocrystalline region produced by ball milling as a function of carbon content. The hardness of the dislocated cell structured region in ball milled powder and martensite[30] are shown for comparison.

2.2 Nanocrystallization by a ball drop test

NS can be produced near the surface of specimens after one or several times of a ball (weight attached) drops. Figure 11[19,31] shows the cross section of the specimen (pearlite structure) deformed by 8 times of ball drops (a weight of 4 kg and a height of 1 m). A dark smooth contrast layer with a thickness of about 15 μm is seen near the surface of the indentation crater. The layer appears at top surface along the edge of crater and appears about 100 μm below the surface at the bottom of the crater. Figure 12 shows a typical dark contrast layer formed in Fe-0.80C specimen with pearlite (Fig. 12(a)) and spheroidite (Fig. 12(b)) structures, respectively. In the dark contrast layer the lamellar structure in pearlite or spherical cementite in spheroidite were disappeared. The microhardness of the dark contrast layer is 10.1 GPa in pearlite and 8.4 GPa in spheroidite, respectively. Those are much higher than the adjacent region with deformed structure (5.8 and 3.6 GPa, respectively). The microhardness and microstructure observed in the dark contrast layers produced by a ball drop test are similar to those observed in ball milled counterparts. Figure 13[31] show TEM bright and dark field (DF) image and the selected area

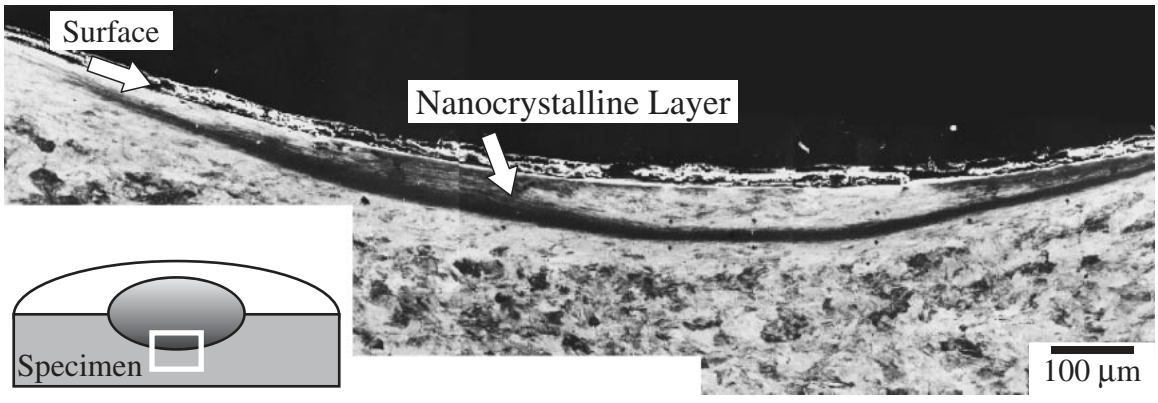

Fig. 11 Nanocrystalline region (dark contrast layer about 15 μm thickness) formed at the surface of specimen (Fe-0.89%C with pearlite structure) by a ball drop test (1 m height, 4 kg weight, 8 times drops).

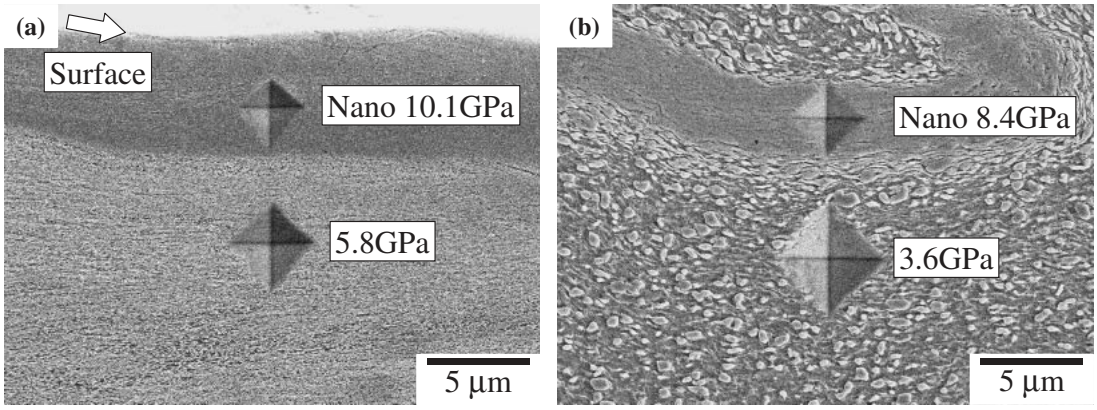

Fig. 12 SEM micrographs showing the hardness of nanograined layer and deformed structured regions. (a) Fe-0.80C pearlite after 70 times ball drops (1 m, 5 kg) and (b) Fe-0.80C spheroidite after 30 times ball drops (1 m, 5 kg).

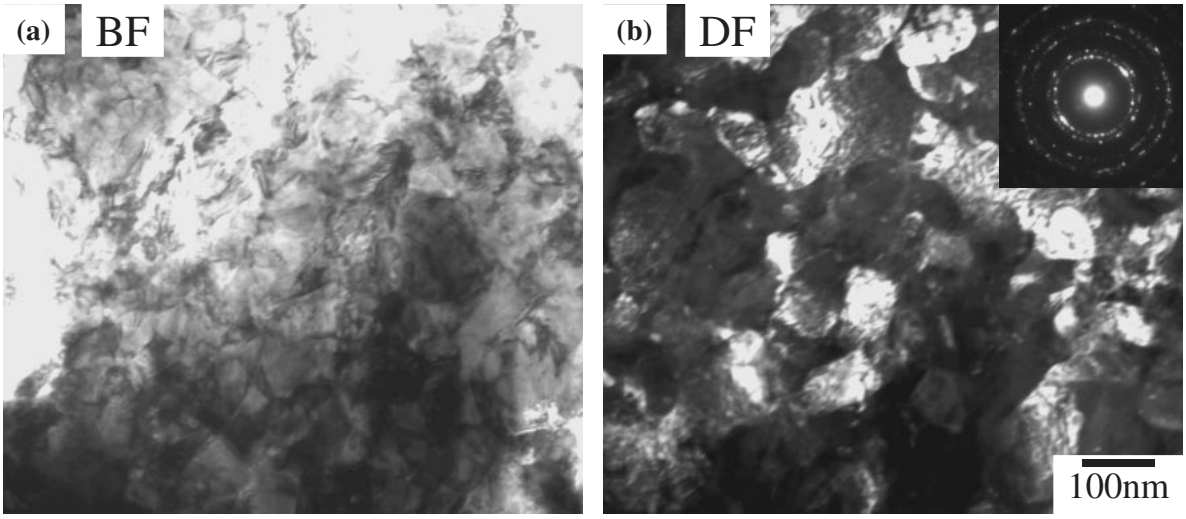

Fig. 13 TEM micrographs of Fe-0.80C pearlite deformed by a ball drop test (1 m, 5 kg, 8 times). (a) bright field image and (b) dark field image of (a) with diffraction pattern (aperture ϕ 1.2 μm).

diffraction (SAD) pattern taken from the dark contrast region of Fe-0.80C specimen with pearlite structure deformed by ball drop test (8 times, 5 kg, 1 m). The TEM DF image shows that the ferrite grain size is about 100 nm and this proves that the dark contrast layer is NS although the grain size is larger than that produced by a long time ball milling. All the diffraction rings in Fig. 13 (b) correspond to bcc ferrite, and rings corresponding to cementite are hardly detected. This indicates that cementite is mostly dissolved into ferrite. The SAD pattern taken from the area of ϕ 1.2 μm shows nearly continuous rings, indicating the random orientations of the ferrite grains.

The amount of strain and strain rate to produce the nanocrystalline layer in a ball drop test were estimated using observed shear bands. Figure 14[19] shows the shear band produced by one time ball trop (5 kg, 1 m) in a pearlitic specimen pre-strained 80% by rolling. From the hardness of the shear band (7.4 GPa), this area was considered as nanostructured region. From the shear angle ($\theta = 7$ degrees) in the picture, the amount of shear strain, γ can be calculated from $\gamma = 1/\tan\theta$ as 8.1 (4.7 in equivalent strain). Taking the pre-strain of 80% rolling reduction (1.9 in true strain) and the uniform 52% thickness reduction (0.7 in true strain) by a ball drop deformation into account, the total true strain of the layer was calculated to be 7.3. This is considered to be the minimum amount of strain to produce NS from the hardness of the shear band. The strain rate was estimated to be around

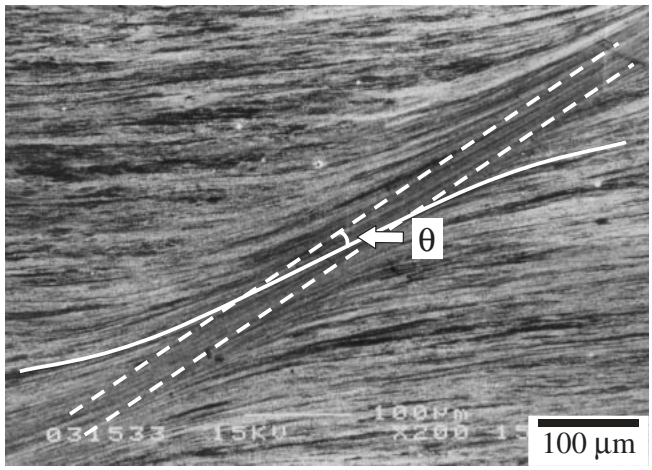

Fig. 14 A shear band with nanograined structure formed in Fe-0.80%C pearlitic steel pre-strained by 80% cold rolling and deformed by one time ball drop (1 m height, 5 kg weight).

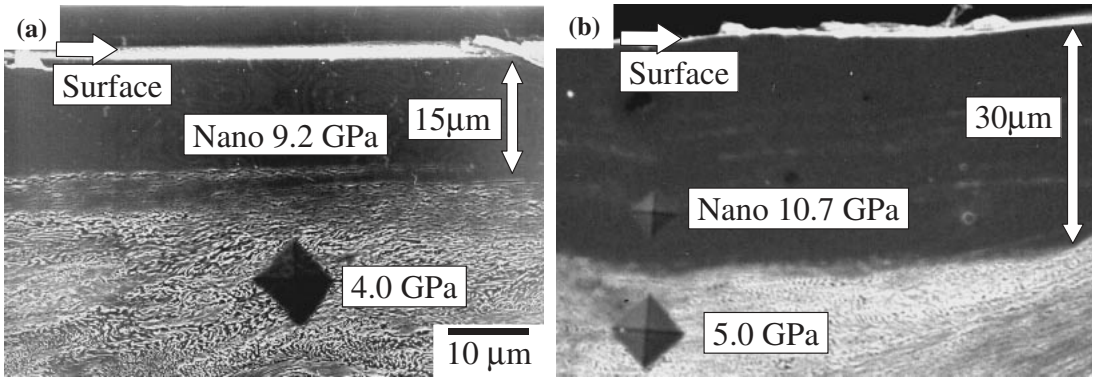

Fig. 15 Temperature effect on the thickness of nanocrystalline surface layer formed by a ball drop test. Fe-0.80%C pearlitic steel was deformed by a ball drop test (1 m height, 5 kg weight, 8 times). (a) at room temperature and (b) at liquid nitrogen temperature.

$10^4\ s^{-1}$ from the ball-to-specimen contact time (4.3×10^{-4} s) and the amount of deformation by one time ball drop (5.4 in equivalent true strain).

The number of ball drops necessary to produce nanocrystalline layer depends on the composition, microstructure and temperature of specimens, and ball drop conditions (weight and height). The number of ball drops is less for harder samples and in higher energy ball drop tests (larger weight and height). Pre-strain of specimen also reduces the number of ball drops. Low processing temperature reduces the number of ball drops to produce nanocrystalline layer or increase the thickness of the nanocrystalline layer if other conditions are being equal. Figures 15 (a) and (b) are SEM micrographs of Fe-0.80C specimen (pearlite structure) after a ball drop test (8 times, 5 kg, 1 m) at R.T. and LN_2 temperature, respectively. It can be seen that under the same ball drop condition the thickness of nanocrystalline surface layer is larger at LN_2 temperature (30 μm) than that at R.T. (15 μm).

2.3 Particle impact experiment

In a particle impact experiment, a hard steel ball of ϕ 4 mm was accelerated by high pressure gas and it impact specimen surface with a speed of 120 m/s. Nanocrystalline region appears as thin layers near specimen surface after several times of particle impacts. Figure 16 shows a typical nanocrystalline layers formed in pearlitic Fe-0.80C specimen after 8 times of particle impacts at LN_2 temperature. The specimen was pre-strained by cold rolling (82%) to enhance nanocrystallization. The dark contrast layer of several 10 μm thickness observed on the top surface was confirmed as nanocrystalline regions by TEM observation. The microhardness of the nanocrystalline region (9.7 GPa) is substantially higher than the subsurface region with deformed structure (4.5 GPa). It was noticed that the microhardness and microstructure of nanocrystalline region produced by particle impact deformation are similar to those observed in specimens after a ball drop test although the layer thickness is slightly thinner.

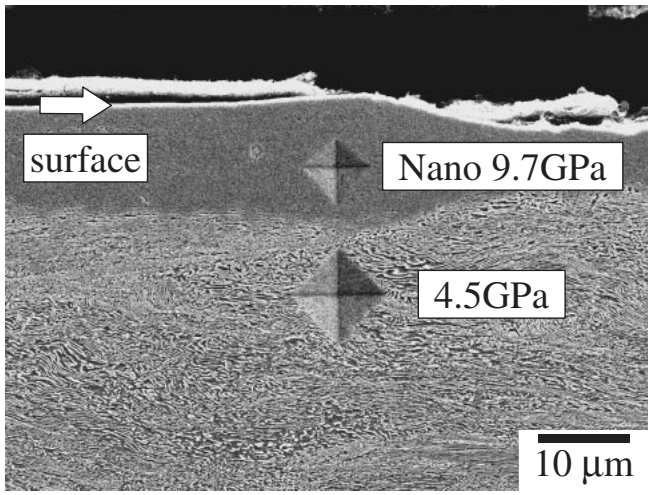

Fig. 16 Nanocrystalline region formed by particle impact deformation (ϕ 4 mm steel ball was projected 8 times with 120 m/s) at liquid nitrogen temperature in Fe-0.80%C pearlitic sample (pre-strained 82% by cold rolling).

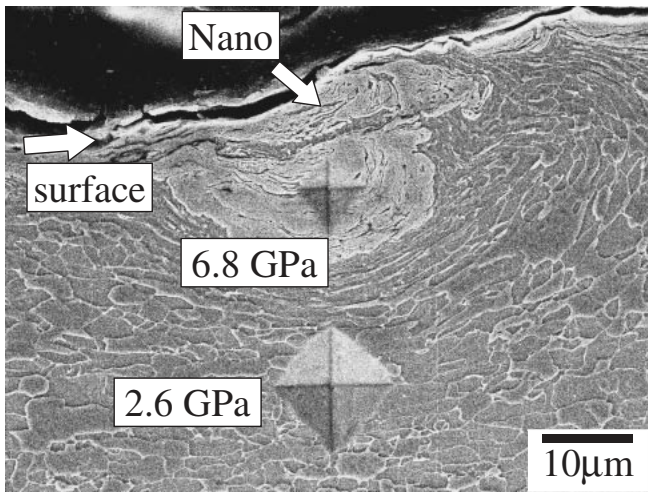

Fig. 17 SEM micrograph showing the nanocrystalline region formed in high tensile strength steel (Fe-0.05%C-1.29%Mn) by shot peening (<50 μm in shot diameter, 190 m/s in shot speed, 10 s of peening time and 1000% in coverage).

2.4 Air blast shot peening

Figure 17 shows a cross sectional SEM micrograph of Fe-0.05C-1.29Mn high tensile strength steel (ferrite structure) after shot peened for 10 s (coverage of 1000%). Again, two

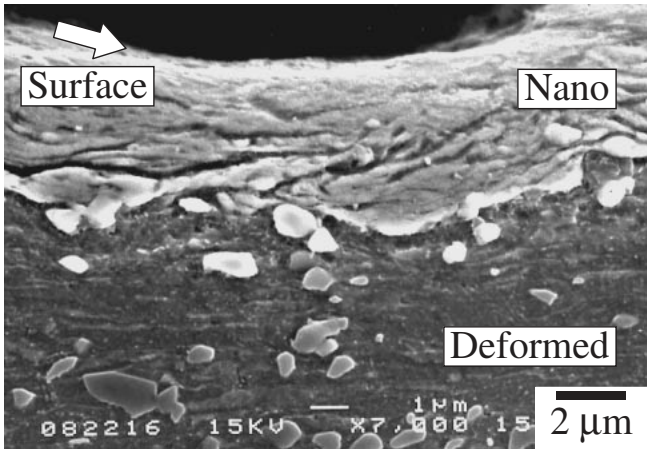

Fig. 18 SEM micrographs showing the nanograined region formed in Fe-0.80%C steel with spheroidite structure (84% cold rolled before shot peening) by shot peening (<50 μm in shot diameter, 190 m/s in shot speed, 10 s in peening time and 1000% in coverage).

distinctive regions can be seen. One is the smooth contrast (nanocrystalline) region near surface with the hardness of 6.8 GPa. Another is the deformed structured region observed at subsurface with the hardness of 2.6 GPa. Figure 18 shows cross section of near surface area of shot peened Fe-0.8C specimen (spheroidite structure pre-strained 84% by cold rolling) after shot peening. Nanocrystalline layer with 5 μm thickness is produced at the top surface. Before shot peening, the spherical cementite particles with diameter about 0.5 μm were uniformly distributed in the ferrite matrix. After shot peening, cementite particles are not visible in the nanocrystalline surface layer. This indicating that the dissolution of cementite takes place in the nanocrystalline layer similar to that observed in ball milled or ball dropped specimens. Figure 19(a) shows nanocrystalline region formed in Fe-3.29Si specimen by 10 s of shot peening (coverage of 1000%). The sharp boundaries are seen between the top surface nanocrystalline layer and subsurface deformed structured region. Figure 19(b) is the TEM dark field (DF) image and selected area diffraction (SAD) pattern of the top surface region of Fe-3.29Si specimen shot peened for 60 s (coverage 6000%). The DF image shows that the ferrite grain size is less than 20 nm, and the SAD pattern indicates that the ferrite grains are randomly orientated.

The production of nanocrystalline surface layer by air blast shot peening has considerable industrial importance since air blast shot peening is a popular process in industries and it can produce nanostructured surface layer with a high productivity. Industrial application of this new technology is expected especially to upgrade the traditional engineering materials.

3. Annealing Behavior of Nanocrystalline Region

The annealing behaviors of nanograined region are quite different from those of the deformed structured region. Figure 20 shows the microstructural change with annealing temperature (annealed for 3.6 ks) in ball milled pure iron (Fe-0.004C). By annealed at 673 K (Fig. 20 (a)), the deformed structured region (lower right) becomes equiaxed grained structure with an average grain size of about 0.5 μm by

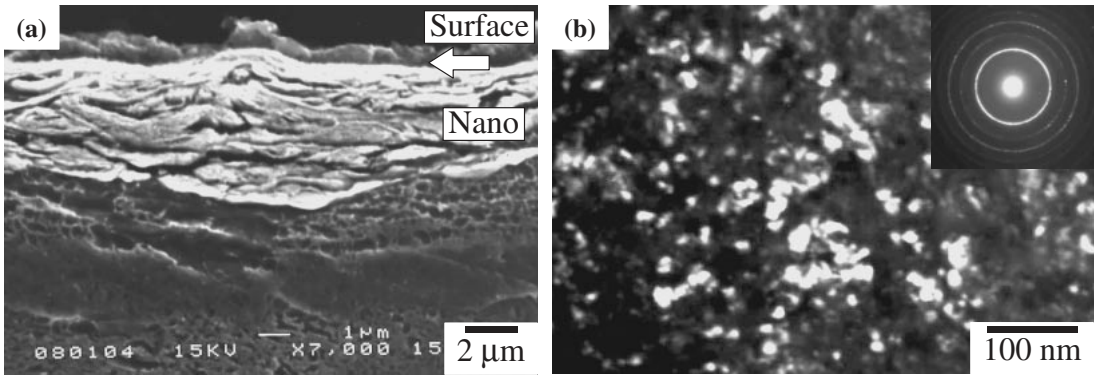

Fig. 19 Micrographs of shot peened (<50 μm in shot diameter, 190 m/s in shot speed) Fe-3.29Si steel. (a) SEM after peened 10 s (1000% in coverage) and (b) TEM (dark field) after peened for 60 s (6000% in coverage). The aperture size of diffraction was ϕ 1.2 μm.

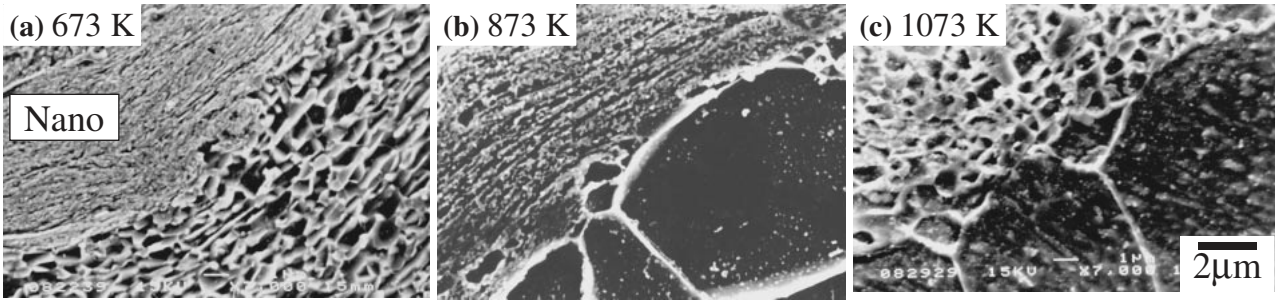

Fig. 20 SEM micrographs of ball milled (for 360 ks) and annealed (for 3.6 ks) pure iron (Fe-0.004C). (a) at 673 K, (b) at 873 K and (c) at 1073 K.

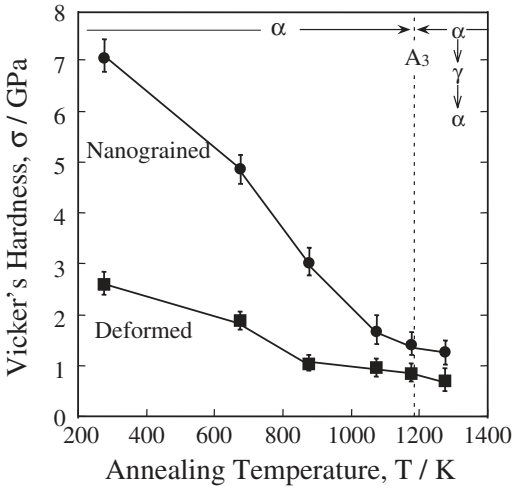

Fig. 21 Microhardness of ball milled (for 360 ks) and annealed (for 3.6 ks) pure iron (Fe-0.004C) as a function of annealing temperature. The hardness of nanograined region and dislocated cell structured regions are measured separately.

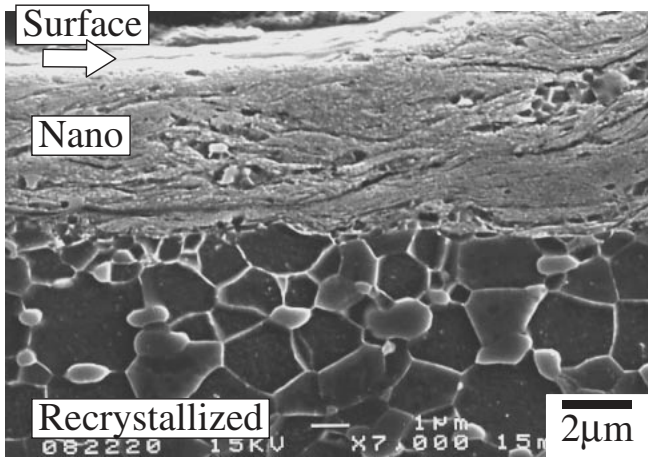

Fig. 22 SEM micrographs showing the annealed structure of Fig. 18. Shot peened Fe-0.80%C spheroidite steel was annealed at 873 K for 3.6 ks.

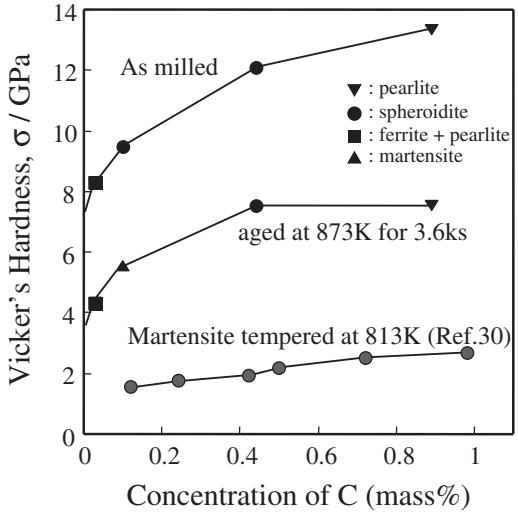

Fig. 23 Microardness of nanocrystalline region in ball milled powder after annealed at 873 K for 3.6 ks as a function of carbon content. The hardness before annealing and that of tempered martensite[30] are shown for comparison.

recrystallization. On the contrary, nanograined structure region showed almost no detectable change (upper left). After annealing at 873 K (Fig. 20 (b)), the recrystallized grain size in the deformed structured region become 10 μm. While, the nanograined region remains almost unchanged. By annealing at 1073 K (Fig. 20 (c)), detectable grain growth to about 0.7 μm occurred in the nanograined region. The change in microhardness of the two regions with annealing temperature is shown in Fig. 21.[32] Comparing the hardness of two regions at each annealing temperature, it is seen that nanograined region has a higher hardness than that of the deformed structured region in all the annealing temperature range. Nanograined region shows a gradual decrease in hardness while deformed structured region shows sharp softening at around 673 K due to recrystallization.

The above difference in annealing behavior in the two regions can be explained as follows. In the deformed (dislocated cell) structured region, conventional recrystallization takes place due to high dislocation density. While, recrystallization does not occur in the nanograined region since almost no dislocations in the interior of grains. It seems that the grain growth of nanograined region is substantially slower than that in a coarse grained counterpart. The slow grain growth rate has been observed in various nanograined materials and it has been suggested that the low mobility of triple junction is responsible.[33,34]

Similar annealing behaviors were observed in the specimens prepared by different methods. Figure 22 shows the annealed structure of shot peened Fe-0.80C sample shown in Fig. 18. After annealed at 873 K for 3.6 ks, nanograined region did not show any detectable change while the deformed structured regions below the nanograined region showed recrystallized structure.

Figure 23[24] shows the hardness of nanograined region produced by ball milling before and after annealing (at 873 K for 3.6 ks) as a function of carbon content. It is seen that the hardness of nanograined region decreases by annealing, but keeps high values of 4.5-8 GPa depending on carbon content. In the figure the hardness of tempered martensite[30] (tempered at 813 K) is shown for comparison. It is clear that the hardness of annealed nanograined region is much higher than those of tempered martesite counterparts.

4. Discussion

4.1 Structural evolution to NS by severe plastic deformation

The evolution of microstructure during low temperature ($<0.5T_m$ (melting temperature)) severe plastic deformation has been the subject of many investigators.[16,35–43] In the deformation at ambient temperature recrystallization during deformation will not take place and recovery is slow. Thus work-hardening continues up to large strains and grains are refined to nanometer range. A general microstructural evolutions at various stages of deformation are as follows. At small strains, original grains are subdivided into cells bounded by dislocation walls (called incident dislocation boundaries (IDBs)) with small misorientation. With increas-

ing strain, cell size and cell wall width decrease and geometrically necessary boundaries (GNBs) develop. GNBs are boundaries which separate a group of neighboring cells with same slip system (called a cell block) from those with different slip systems. With further increase in strain, the density of GNBs and the misorientation of GNBs increase. Since the deformation induced high angle boundaries thus produce contain high density of dislocations and are distorted elastically, they are called non-equilibrium grain boundaries.[42,43] The dislocation density inside grains is low in spite of the large strain imposed.[43] When the grains are refined to 10 nm range, the microstructure reaches a steady state since further strains are mainly accommodated by grain boundary sliding.[39] By annealing, the NS produce by severe plastic deformation does not recrystallize and show substantially slow grain growth.[27–29]

The observed microstructural evolution and grain refinement during heavy deformation up to submicron range reported by many workers agree well each other. Regarding grain refinement to nanometer range, there are two types of results. One is continuous or gradual decrease in grain size to nanometer range and another is sudden change in grain size with strain. The first case is typically shown by Hughes and Hansen.[40] They observed the surface layers of the Cu friction samples. The boundary spacing of 12 nm was observed at the top surface. The boundary spacing continuously increases with the depth from 12 nm to 80 nm at 4 μm and several microns at 100-200 μm below the surface. From the morphological similarity observed in friction and rolling, they suggested that same underlying slip and shear mechanisms are controlling the microstructure evolution from grain/cell size of several μm to 10 nm. The latter case is that observed in ball milling,[27–29,32] shot peening[24] and wear test.[18,41] Heilmann *et al.*[41,42] observed wear sample treated by block-on-ring sliding test. A surface layer (called transfer layer) with grain size of ~3-30 nm was observed. It was suggested that the mixing with counterface material and/or environmental components produces the nanograined transfer layers. The thickness of transfer layers may range from several to tens of μm. The adjacent region consists of subgrains and cells of 0.2-0.4 μm range. The transfer layer and the block materials below it are separated by a sharply defined interface. The formation mechanism of the sharply defined boundaries is discussed below.

4.2 Deformation conditions to produce nanocrystalline structure

To optimize the known processes or develop new processes to produce NS, it is important to understand the necessary and favorable conditions to produce NS. The amount of strain, strain rate and other favorable conditions to produce Ns are considered.

4.2.1 Amount of strain

Impose a large strain seem to be the most important condition to produce NS. The reported amount of strain applied to obtain NS (grain size less than 100 nm) varies from 7 to 31 depending on the deformation techniques and materials employed.

The amount of strain can be measured well in drawing and torsion experiments. Langford and Cohen[35] observed microstructure of severely drawn iron wire strained up to $\varepsilon = 6$. After straining to $\varepsilon = 6$ the flow stress increased to 1.4 GPa and mean transverse linear-intercept cell sizes reduced to 90 nm. If it is assumed that 1.4 GPa is simply due to grain boundary strengthening, the size of grains (with medium and large misorientation) is estimated to be 260 nm according to the Hall-Petch relationship for iron[32] (*i.e.*, σ [GPa] = $0.12 + 20d^{-1/2}$, d in nm). Extrapolating their flow stress vs strain data, the strain which gives the flow stress corresponding to $d = 100$ nm (2.1 GPa) is estimated to be $\varepsilon = 12$. Tashiro[44] measured the flow stress of drown iron wire strained up to $\varepsilon = 11.5$. The flow stress increased linearly with strain and reached 3 GPa at a strain of 11. The flow stress corresponding to $d = 100$ nm (2.1 GPa) is achieved at $\varepsilon = 7$. Although the grains size of the drown wire was not measured, grain size less than 100 nm is believed to be accomplished. The experiment of high pressure torsion straining in iron was carried out by Valiev *et al.*[16] Armco iron was subjected to torsion straining up to 10 turns ($\varepsilon = 360$) under a pressure of 7 GPa at a strain rate of $0.5\ s^{-1}$. They reported that the grain size decreased and hardness increased with increasing strain. After 3 turns ($\varepsilon = 108$) the hardness reaches 4.5 GPa and tends to reach a steady state. The grain size about 100 nm was obtained after 5 turns ($\varepsilon = 180$) at which the hardness was 4.6 GPa. The microhardness of 4.6 GPa corresponds to the flow stress of 1.53 GPa from the usual approximate relation between microhardness and flow stress, namely $Hv = 3\sigma$. The reported hardness is too low to consider that the size of grains with large misorientation is reduced to 100 nm in their experiment. Similar torsion experiment has been done by Kaibyshev *et al.*[17] in Fe-3%Si under the pressure of 9 GPa. After straining to $\varepsilon = 31$ (0.5 turn), grains are reduced to 120-200 nm and the microhardness increased to 7.2 GPa. From the obtained microhardness it can be considered that the grain size less than 100 nm was achieved. The hardness measured was 3.6 GPa at $\varepsilon = 4.3$ and 7.2 GPa at $\varepsilon = 31$, then the grain refinement to $d = 100$ nm (Hv = 6.3 GPa) is expected to be accomplished at a strain $4.3 < \varepsilon < 31$.

The amount of strain to produce nanocrystalline structure was also estimated in a BD test and sliding wear test, although with less accuracy. In a ball drop test of pearlitic steel, Umemoto *et al.*[45] estimated $\varepsilon = 7.3$ at strain rate of around $1.3 \times 10^4\ s^{-1}$. In sliding wear test, Heilmann *et al.*[42] obtained nanograined layer of 3-30 nm on the top surface of Cu block. The estimated plastic shear strain at the surface was ~11.4 and the strain rate was $<3.7 \times 10^3\ s^{-1}$. Hughes and Hansen[40] studied the nanostructures in Cu produced by sliding. The amount of strain to reach $d = 100$ nm is estimated from the relationship between grain size (or grain boundary spacing) and strain as 8.

Summarizing the above mentioned studies, the minimum amount of strain necessary to produce nanocrystalline structure is considered to be around $7 \sim 8$, although it depends on materials, microstructure, deformation techniques and deformation conditions employed.

4.2.2 Strain rate

High strain rate deformation may not be a necessary condition to produce NS but it probably enhance the formation due to the following several reasons: (1) increase flow stress, (2) increase work-hardening at a given strain, (3)

increase dislocation multiplication rate, and (4) promote lattice rotation and increase misorientation angle.

It has been well known that flow stress of metals increase with strain rate.[46] Higher flow stresses activate a larger number of slip systems and promote grain subdivision and subgrain rotation. Greater hardening has been observed in metals strained at higher strain rates when compared at equal strain. The iron samples subjected to high-intensity shock waves of explosive origin (strain rate $\sim 10^6\,s^{-1}$) showed much greater hardening than those deformed by rolling.[47] Thus it is expected that high strain rate deformation reduce the necessary amount of strain to produce NS. High strain rate deformation promote smaller cells or subgrains due to higher dislocation multiplication rate and hence higher dislocation density than those deformed at low strain rates. The rotation of cells or grains is induced by the deformation of different slip systems in adjacent cells or grains. Since high strain rate deformation activate more slip systems due to high flow stress, high strain rates are favorable to obtain randomly oriented fine grains with large misorientation.

As the strain rate is increased the deformation tends more and more towards an adiabatic state. The generated heat rise the temperature of sample and accelerates recovery and grain growth. In an extreme case the increase in strain rate results in the increase in grain size.[48] Thus to obtain grain refinement by high strain rate deformation, care should be taken for cooling during and post deformation so that the temperature of the specimen will not rise so much.

4.2.3 Other deformation factors

Other favorable conditions for the formation of NS are considered as follows; (1) low temperature deformation, (2) hydrostatic pressure, (3) repetitive or cyclic deformation, (4) multidirectional deformation, (5) impurities, alloying elements and second phase.

The suppression of recovery by preventing dislocation motion favors the formation of NS. Low deformation temperature and hydrostatic pressure slow down self-diffusion and, consequently, delay recovery kinetics. Applying a large accumulative strain by cyclic or repetitive deformation with a small strain at each time is effective to suppress recovery since specimens are cooled during each strain interval. Multidirectional deformation activates multi slip systems and increases dislocation interaction frequencies which leads to the development of fine cells. Impurities, alloying elements, precipitates and second phase disturb dislocation motion and suppress recovery.

4.3 Clear boundaries separate nanograined region

Clear boundaries which separate nanograined region from deformed structured region shown typically in Fig. 4 were commonly observed in ball milling, a ball drop test, particle impact experiment and shot peening. However, in most of the previous studies, clear boundaries have not been observed and the refinement of cells or grains by deformation has been considered to be a continuous process. The possible causes of the formation of sharply defined boundaries are; (1) impurities, (2) martensitic transformation, (3) unique deformation mode, (4) common phenomena in deformation. The effect of impurity has been discussed regarding the sharp boundaries observed in ball milled powder.[32] In ball milling contamination from balls, vials and environmental gases occurs. The powder surface with higher impurity concentration becomes NS and interior of powder with lower impurity content remains as deformed cell structure and clear boundaries appear between them. Impurities retards dislocation motion and certain elements segregate to grain boundaries, reduce grain boundary energy and promote nanocrystallization. However, clear boundaries were observed in specimens treated by a ball drop test or shot peening where contamination is hard to occur. Thus it is considered that impurity alone cannot be a reason of the clear boundaries although it might help. The second possible reason of the formation of clear boundaries is martensitic transformation. This idea is that nanograined region formed by martensitic transformation is separated with clear boundary from the deformed structured region without martensitic transformation. When specimens received large strains at high strain rates, the temperature of the specimen rise substantially. If the temperature rises above A_1 or A_3 point, the transformation to austenite phase can occurs. During unloading, the temperature of austenite area decreases rapidly and transforms to martensite. The martensitic transformation during cooling of the adiabatically deformed materials have been observed on the rail surface and called "white etching layer".[49] However, the nanograined regions produced in carbon steels exhibit much higher hardness than that of martensite with same carbon content. Furthermore, as observed in a ball drop test when specimens are deformed at liquid nitrogen temperature, the nanograined layer thickness become larger than that produced at room temperature. Nanograined region also forms in Fe-3%Si alloy where the bcc phase is stable up to its melting temperature. From those reasons, it is hard to accept that thermally induced fcc to bcc martensitic transformation is responsible for the observed clear boundaries. Another possible martensitic transformation is bcc to hcp transformation by hydrostatic pressure. In iron, bcc to hcp transformation takes place around 11.0-11.5 GPa at room temperature.[50] According to the Hertzian elastic contact theory,[51] when a spherical particle impact a semi-infinite specimen with the speed of 100 m/s, the maximum pressure is 15 GPa. Thus in steels pressure induced martensitic transformation from bcc to hcp can occur when a high velocity particle impact a specimen. During unloading, the hcp structure re-transform to bcc martensitically. Although martensitic transformation alone cannot produce nanocrystallization but martensitic transformation produces irreversible lattice defects and reduce the amount of strain to reach nanocrystalline state. The unique deformation mode can be another reason of clear boundaries. In ball milling, a ball drop test, particle impact deformation or shot peening, the strain is highly concentrated near specimen surface. The amount of strain and strain rate is a strong function of depth from the surface. Thus it can be considered that the clear boundary may corresponds to drastic change in the strain or strain rate. However, strain or strain rate in a material changes continuously with distance and hard to consider they change such abruptly. Furthermore various amount of strains are given at various strain rates in the processes studied but intermediate structure between nanocrystalline and dislocated cell structures has never been observed. The last proposed

idea is to consider that the sharp transition from dislocated cell to nanocrystalline structure is common phenomena in deformation and this occurs irrespective of materials or mode of deformation. However, gradual change in grain size to nanometer range has been observed[40] and it is hard to accept that sharp change is a common behavior of deformed material. From the above discussion on the formation mechanisms of the clear boundaries between nanograined and dislocated cell structures, it is suggested that several reasons may contribute simultaneously. The real mechanism is still not clear and further investigations are needed.

5. Summary and Conclusions

In the present paper, the formation of nanograined structure by various severe plastic deformation were demonstrated. The general microstructural changes during severe deformation observed were reviewed. The conditions to produce nanograined structure were discussed. The main contents are summarized as follows.

(1) In ball milling, nanograined structure was obtained in steels irrespective of the carbon content and starting microstructure. The nanograined regions appear near the surface of powder and are separated from the interior deformed structured region with sharp boundaries. The hardness of nanograined region is extremely high and increases with carbon content from 7 to 13 GPa. The cementite (either lamellar or spherical) dissolves completely by ball milling when the nanocrystallization of ferrite matrix starts.

(2) In a ball drop test and particle impact deformation, similar nanograined structure was obtained in the surface layer after several times of impact. Deformation at liquid nitrogen temperature enhanced the formation of nanograined region.

(3) In air blast shot peening, nanograined structure is produced when larger coverage ($>1000\%$) and higher shot speed ($>100\,m/s$) than conventional operation are applied.

(4) By annealing, nanograined structured region showed substantially slow grain growth without recrystallization.

(5) The microstructure change from dislocated cell to nanograined structure during severe plastic deformation occurs either gradually or discontinuously depending on a process employed.

(6) To produce nanograined structure by deformation, the most important condition is to impose a large strain (larger than about 7). High strain rates, low temperature deformation, multidirectional deformation, hydrostatic pressure are considered to be favorable conditions to produce nanograined structure.

(7) The mechanisms of the formation of sharply defined boundaries which separate nanograined region from dislocated cell structured region were discussed with respect to impurities, martensitic transformation and deformation mode. It was suggested several mechanisms may operate simultaneously in the formation of the clear boundaries.

Acknowledgements

This work is partly supported by the Grant-in-Aid by the Japan Society for the Promotion of Science. The author thanks Dr. K. Tsuchiya, Dr. Y. Todaka for their involvement.

REFERENCES

1) I. Tamura, H. Sekine, T. Tanaka and C. Ouchi: *Thermomechanical Processing of High-strength Low-alloy Steels*, (Butterworths, 1988).
2) M. Niikura, Y. Hagiwara, K. Nagai, K. Tsuzaki and S. Takaki: Proc. of Int. Symp. on Ultrafine Grained Steels, (The Iron and Steel Inst. of Japan, 2001) 26-33.
3) V. M. Segal, V. I. Reznikov, A. D. Drobyshevskiy and V. I. Kopylov: Russ. Metall. **1** (1981) 99-105.
4) R. Z. Valiev, N. A. Krasilnikov and N. K. Tsenev: Mater. Sci. Eng. A **137** (1991) 35-40.
5) R. Z. Valiev, A. V. Korznikov and R. R. Mulyukov: Phys. Met. Metall. **73** (1992) 373-383.
6) Y. Saito, N. Tsuji, H. Utsunomiya, T. Sakai and R. G. Hong: Scr. Mater. **39** (1998) 1221-1227.
7) Y. Saito, H. Utsunomiya, N. Tsuji and T. Sakai: Acta Mater. **47** (1999) 579-583.
8) H. Gleiter: 2nd Riso Int. Symp. Metall. and Mat. Sci., eds. N. Hansen, A. Horsewell and H. Lilholt (Riso National Laboratory, Denmark, 1981) 15-21.
9) L. Lu, M. L. Sui and K. Lu: Science **287** (2000) 1463-1466.
10) G. Plumbo, S. J. Thorpe and K. T. Aust: Scr. Metall. Mater. **24** (1990) 1347-1350.
11) Y. Yoshizawa, S. Oguma and K. J. Yamaguchi: J. Appl. Phys. **64** (1988) 6044-6046.
12) P. H. Shingu, B. Huang, S. R. Nishitani and S. Nasu: Proc. of JIMIS-5, Non-Equilibrium Solid Phases of Metals and Alloys **29** (1988) 3-10.
13) J. S. C. Jang and C. C. Koch: Sri. Metal. **24** (1990) 1599-1604.
14) H. J. Fecht, E. Hellstern, Z. Fu and W. L. Johnson: Metall. Trans. **21A** (1990) 2333-2337.
15) J. Eckert, J. C. Holzer, C. E. Krill, III and W. L. Johnson: J. Mater. Res. **7** (1992) 1751-1761.
16) R. Z. Valiev, Y. V. Ivanisenko, E. F. Rauch and B. Baudelet: Acta Mater. **44** (1996) 4705-4712.
17) R. Kaibyshev, I. Kazakulov, T. Sakai and A. Belyakov: Proc. of Int. Symp. on Ultrafine Grained Steels, (The Iron and Steel Inst. of Japan, 2001) 152-155.
18) P. Heilmann, W. A. T. Clark and D. A. Rigney: Acta Metall. **31** (1983) 1293-1305.
19) M. Umemoto, B. Haung, K. Tsuchiya and N. Suzuki: Scr. Mater. **46** (2002) 383-388.
20) M. Umemoto, X. J. Hao, T. Yasuda and K. Tsuchiya: Mater. Trans. **43** (2002) 2536-2542.
21) N. R. Tao, M. L. Sui, J. Ku and K. Lu: NanoStructured Mater. **11** (1999) 433-440.
22) I. Altenberger, B. Scholtes, U. Martin and H. Oettel: Mater. Sci. Eng. A **264** (1999) 1-16.
23) X. Y. Wang and D. Y. Li: Wear (2003) **255** (2003) 836-845.
24) M. Umemoto, Y. Todaka and K. Tsuchiya: Mater. Trans. **44** (2003) 1488-1493.
25) D. A. Konstantinidis and E. C. Aifantis: NanoStructured Mater. **10** (1998) 1111-1118.
26) C. K. Rhee, G. H. Lee, W. W. Kim, V. V. Ivanov, S. V. Zajats and A. I. Medvedev: J. of Metastable and Nanocrystalline Mater. **15-16** (2003) 401-406.
27) Y. Xu, Z. G. Liu, M. Umemoto and K. Tsuchiya: Metall. Mater. Trans. **33A** (2002) 2195-2203.
28) Y. Xu, M. Umemoto and K. Tsuchiya: Mater. Trans. **43** (2002) 2205-2212.
29) M. Umemoto, Z. G. Liu, K. Masuyama, X. J. Hao and K. Tsuchiya: Scr. Mater. **44** (2001) 1741-1745.
30) G. Krauss: *Steel: Heat Treatment and Processing Principles*, (ASM Int., 1990).
31) Y. Todaka, M. Umemoto and K. Tsuchiya: ISIJ Int. **42** (2002) 1430-1437.
32) J. Yin, M. Umemoto, Z. G. Liu and K. Tsuchiya: ISIJ Int. **41** (2001) 1391-1398.
33) C. H. Moelle and H. J. Fecht: Nanostruct. Mater. **6** (1995) 421-424.
34) T. R. Marlow and C. C. Koch: Acta Mater. **45** (1997) 2177-2186.
35) G. Langford and M. Cohen: Trans. ASM **62** (1969) 623-638.
36) D. A. Hughes and N. Hansen: Acta Mater. **48** (2000) 2985-3004.

37) N. Tsuji, R. Ueji, Y. Ito and Y. Saito: Riso Int. Symp. (2000) 607-616.
38) A. Belyakov, T. Sakai, H. Miura and R. Kaibyshev: Philos. Mag. Lett. **8** (2000) 711-718.
39) K. Lu and J. Lu: Mater. Sci. Eng. A (2003) in press.
40) D. A. Hughes and N. Hansen: Phys. Rev. Lett. **87** (2001) 135503-1-131550-04.
41) P. Heilmann, J. Don, T. C. Sun and D. A. Rigney: Wear **91** (1983) 171-190.
42) R. Z. Valiev: Proc. of Int. Symp. on Ultrafine Grained Steels, (The Iron and Steel Inst. of Japan, 2001) 52-57.
43) R. Z. Valiev, R. K. Islamgaliev and I. V. Alexandrov: Mater. Sci. **45** (2000) 103-189.
44) H. Tashiro: Doctor thesis at Tohoku Univ. (1992).
45) M. Umemoto, Y. Todaka and K. Tsuchiya: Mater. Sci. Eng. A (2003) in press.
46) J. D. Campbell and W. G. Ferguson: Philos. Mag. **21** (1970) 63-82.
47) G. E. Dieter: *Response of metals to high velocity deformation*, eds. P. G. Shewman and V. F. Zackay, (Interscience, New York, 1961) 409-445.
48) N. Tsuji, T. Toyoda, Y. Minamino, Y. Koizumi, T. Yamane, M. Komatsu and M. Kiritani: Mater. Sci. Eng. A (2003) in press.
49) W. Osterle, H. Rooch, A. Pyzalla and L. Wang: Mater. Sci. Eng. A **303** (2001) 150-157.
50) H. G. Drickamer: Rev. Sci. Instrum. **41** (1970) 1667-1668.
51) S. T. S. Al-Hassani: Proc. 1st Int. Conf. on Shot Peening, (Paris, 1981) 583-602.